First-principles study of the composition, structure, and stability of the FeO (111) surface

Y. L. Li,[1] K. L. Yao,[1,2,3,*] Z. L. Liu,[1,†] and G. Y. Gao[1]
[1]*Department of Physics, Huazhong University of Science and Technology, Wuhan 430074, People's Republic of China*
[2]*International Center of Materials Physics, The Chinese Academy of Science, Shenyang 110015, People's Republic of China*
[3]*CCAST (World Lab), P. O. Box 8730, Beijing 10080, People's Republic of China*
(Received 15 June 2005; revised manuscript received 18 August 2005; published 31 October 2005)

We performed systematic full-potential density functional theory studies on all possible (1×1) terminations of the low-index surface (111) of FeO with NaCl ($B1$) phase and inverse NiAs ($iB8$) phase, respectively. Applying the concept of first-principles atomistic thermodynamics, we analyze the composition, structure, and stability of the FeO (111) orientation in equilibrium with an arbitrary oxygen environment. The density of states (DOS) of the relaxed FeO (111) surface with $B1$ structure and inverse $B8$ ($iB8$) structure within the studied subset of (1×1) geometries were calculated and compared with the DOS of the bulk FeO with the two structures. The calculations reveal that the (111) surfaces of FeO($B1$)-Fe and FeO($B1$)-O have metallic and ferromagnetic properties, and they are different from those of the bulk of FeO ($B1$). While the (111) surfaces of FeO($iB8$)-Fe and FeO($iB8$)-O show semiconducting and antiferromagnetic properties similar to those of the bulk of FeO($iB8$).

DOI: 10.1103/PhysRevB.72.155446 PACS number(s): 73.20.At, 75.70.Rf, 68.47.De, 68.47.Fg

I. INTRODUCTION

Metal oxide is of high current interest due to its many technologically important uses, such as catalysis, magnetic data storage, high-temperature superconductivity, and the colossal magnetoresistive materials.[1–4] To obtain a microscopic understanding of these compounds, it is necessary to know their surface atomic structure, which is also influenced by temperature and partial pressures in the environment. This can be particularly important for oxygen containing environments, where the stability of different surface terminations of varying stoichiometry may well be anticipated as a function of oxygen in the surrounding gas phase. The transition-metal monoxides, with the rock salt $B1$ structure at ambient condition, have occupied a special position in condensed-matter physics for decades as a prototypical example of the Mott insulators.[5–7] For FeO, its stability of surface may have an important implication in the surface science because FeO is one of the basic oxide components in the interior of the Earth.[8,9] The antiferromagnetic (AF) spin ordering is such that all transition-metal ions in planes perpendicular to the (111) direction of the rock salt cell have the same spin alignment, and the spins between nearest-neighboring planes are antiparallel. On the other hand, the $iB8$ phase of transition-metal compounds was first mentioned in the work by Cohen *et al.*,[10,11] and then Fang *et al.* proved that the $iB8$ phase with the AF ordering is uniquely so stable as the high-pressure structure of FeO.[12] So we will discuss the (111) surface of FeO with the $B1$ phase and the inverse $B8$ ($iB8$) phase, respectively.

II. COMPUTATIONAL METHOD

The calculations were performed in the framework of density functional theory (DFT). We employed the full potential linearized augmented plane wave (FPLAPW) method as implemented in the WIEN2K package[13] and the local-density approximation (LDA)+U calculation[14,15] with the "SIC" double-counting recipe, which is appropriate for strongly localized electrons. At the same time, the spin-orbit coupling was taken into account to supplement the generalized gradient approximation (GGA) results. In this LDA+U method, the strong correlation between localized d-electrons is explicitly taken into account through the screened effective electron-electron interaction parameter $U_{\mathrm{eff}}=U-J$ with U and J denoting the Coulomb and exchange integral, respectively.

In our case, the self-consistent field calculations are based on the structural parameters: the atomic-sphere radii R_{mt} are chosen as 2.3 and 1.7 a.u. for the Fe and O atoms, respectively. The cutoff parameter $R_{mt}K_{\max}$ for limiting the number of the plane waves is equal to 8.5, where $K_{\max}$ is the maximal value of the reciprocal lattice vector used in the plane wave expansion, and R_{mt} is the smallest atomic-sphere radius in the surface cell. So the plane-wave cutoff energy is 340 eV. In the atomic-sphere regions, the basis set consists of spherical harmonics with azimuthal quantum number $l\leqslant10$, and nonspherical contributions of the charge density and potential with $l\leqslant5$, and the charge density was Fourier expanded up to $G_{\max}=14$. For the Brillouin zone integration, we used 500 k points in the whole first Brillouin zone (20 k points in the irreducible part of the surface Brillouin zone) and 205 plane waves at the equilibrium lattice constant. This set of parameters ensures a total energy convergence of 3.3×10^{-5} eV per atom. The convergence was also checked by further increasing the cutoff energy and the k-points density. We performed supplementary LDA+U calculations, which have been regarded as one way to treat the system with strong correlation. Screened Coulomb U and exchange J integrals enter the LDA+U energy functional as external parameters and have to be determined independently. In principle, their values can be obtained from LDA calculations using Slater's transition state approach.[16] At the same time, to identify the U and J values, we also consulted some related references about the choice of the empirical U and J values of FeO,[14,17] and then we used the value of $U=5.3$ eV and $J=1.0$ eV, which is to say $U_{\mathrm{eff}}=4.3$ eV. All the

parameters we chose were kept fixed during our calculations.

III. RESULTS OF SURFACE CALCULATIONS

To simulate the (111) surface of FeO, we use supercells containing 7–11 layers and 10 Å vacuum above the (111) surface. The outermost 2–4 layers are fully relaxed for the surface. We have also performed test calculations with thicker slabs and relaxing more layers, and we have restricted the calculations to structures compatible with a (1×1) cell.

Usually, FeO adopts a rhombohedrally NaCl-structure ($B1$) at low pressures and temperatures approaching 0 K. The local magnetic moments on the Fe ions are responsible for the insulating behavior of FeO, as demonstrated by optical spectroscopy and by *ab initio* calculation.[18,19] In addition, the high-pressure phase of $Fe_{1-x}O$ was recently assigned to be the NiAs ($B8$) type structure by the analysis of x-ray diffraction peak position.[20,21] On the analogy of most of the transition-metal compounds with the $B8$ structure, a natural idea for the $B8$ FeO may be such that Fe occupies the Ni site and O the As site. This structure is named normal $B8$ ($nB8$ for short) hereafter. However, another structure, which is named inverse $B8$ ($iB8$), is possible by exchanging the Fe and O positions. The two structures are different in general and, moreover, have different symmetries for the AF order case. To the best of our knowledge, no transition-metal compounds have ever been known to take the $iB8$ structure. Actually, the intensity profile of the observed x-ray diffraction pattern for $Fe_{1-x}O$ is not consistent with the $nB8$ structure, though both structures will give the same x-ray diffraction peak positions if the lattice parameters are the same. The $iB8$ phase was first mentioned in the work by Cohen *et al.*[10] without any judgment on the relative stability between the $nB8$ and $iB8$ phase. Subsequently, Fang *et al.* proved that

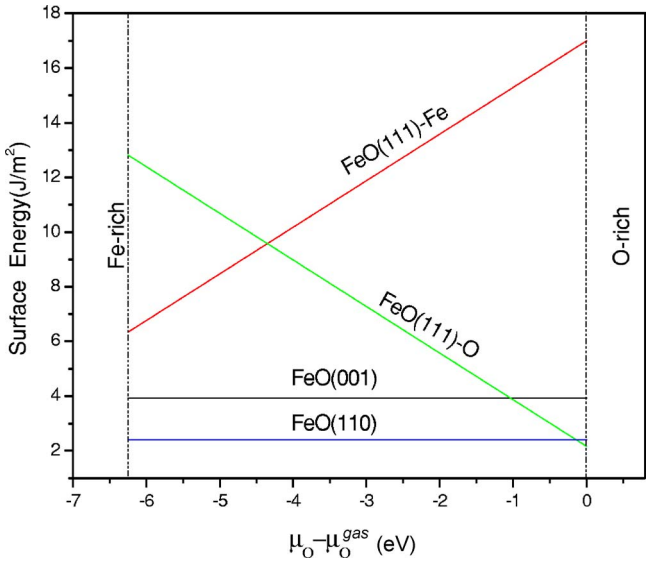

FIG. 1. (Color online) Surface energies ($B1$ phase) of the Fe-terminated and O-terminated FeO(111) and FeO (001) (110) vs $\mu_O - \mu_O^{\text{gas}}$. The FeO(111)-Fe and FeO(111)-O present the Fe-terminated and O-terminated FeO(111) surface, respectively.

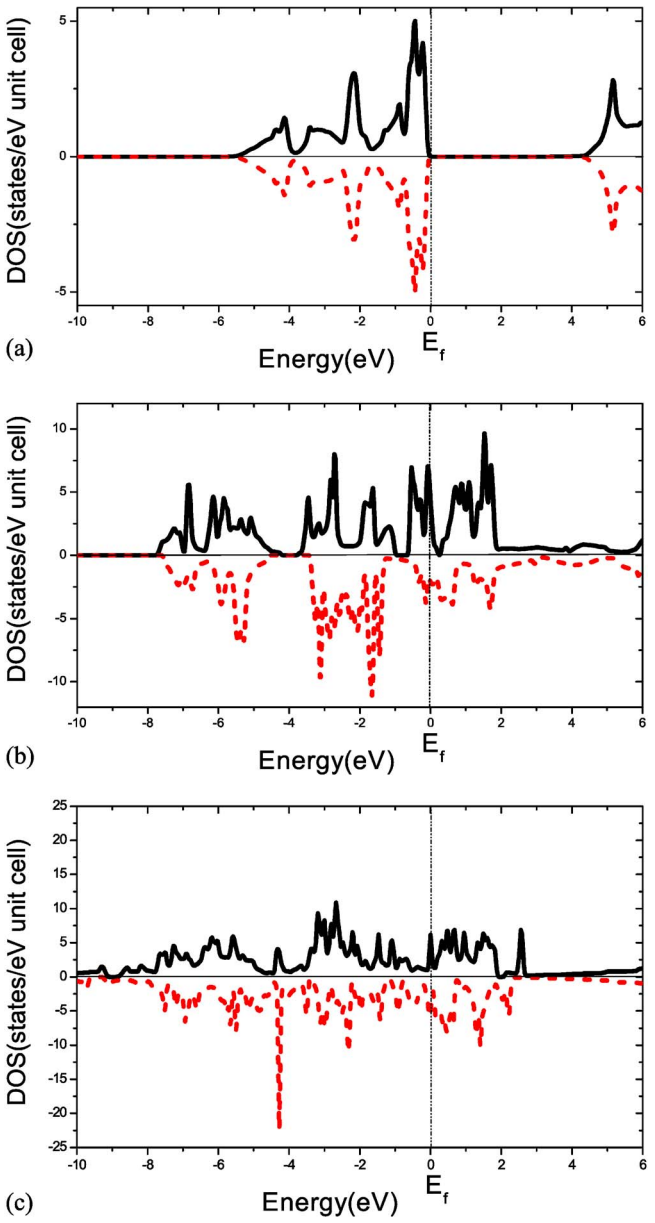

FIG. 2. (Color online) Density of states for (a) the relaxed bulk of FeO ($B1$), (b) FeO($B1$)-Fe (111) surface, (c) FeO(B1)-O (111) surface (dark solid: spin-up states; red dashed: spin-down states; dotted: the Fermi level).

$iB8$ phase is more stable than $nB8$ phase for FeO under high pressure.[12] So in this paper, we will discuss the stability of FeO(111) surface with the $B1$ and $iB8$ phase.

Within our DFT-GGA approach, the optimized lattice constants of the FeO ($B8$B1 structure) unit cell are obtained as $a = 3.016\,849$ Å, which is in reasonably good agreement with the experimental lattice constants, $a_{\text{exp}} = 3.063\,187$ Å. The FeO (111) surface is characterized by alternating layers of Fe and O atoms along the direction normal to the surface forming, therefore, either a completely Fe [FeO(111)-Fe] or a completely O [FeO(111)-O] terminated surface. In the following, we will compare the (001) (110) surface energy with the (111) polar surface, and the stability issue will also be discussed in more detail. For the $iB8$ phase of FeO, there is

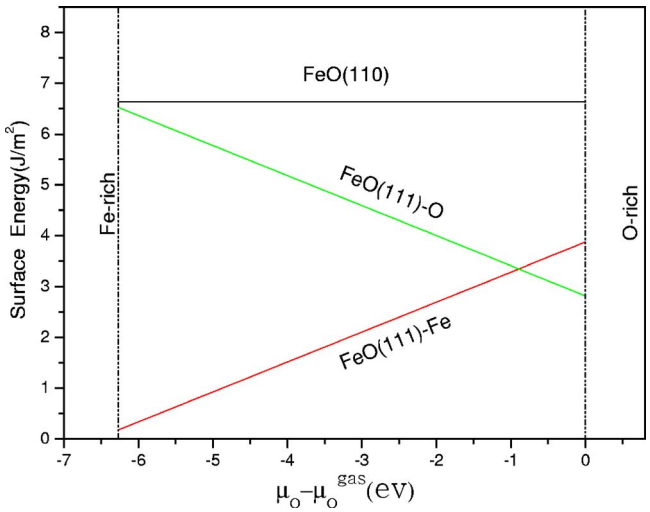

FIG. 3. (Color online) Surface energies (*iB*8 phase) of the Fe-terminated and O-terminated FeO(111) and FeO (110) vs $\mu_O - \mu_O^{\text{gas}}$. The FeO(111)-Fe and FeO(111)-O present the Fe-terminated and O-terminated FeO(111) surface, respectively.

not any experimental information about the structure and composition of crystalline FeO surfaces available from the experimental side, so we used the optimized lattice constant $a=b=2.517\,005$ Å, $c=5.673\,125$ Å. The surface free energy of polar surface (111) (*iB*8 phase) was studied and compared with the (110) surface.

To compare the relative stability of structures containing different numbers of atoms, we consider different surfaces in contact with an oxygen atmosphere described by oxygen pressure P and temperature T. The surface energy of the corresponding system σ can be given by[22–25]

$$\sigma = (E_{\text{tot}} - N_{Fe}\mu_{Fe} - N_O\mu_O - PV - TS)/A. \quad (1)$$

Here, E_{tot} is the total energy of the slab, and μ_{Fe} and μ_O are the chemical potentials of Fe and O, respectively. In addition, N_{Fe} and N_O are the numbers of the corresponding atoms in the slab. A is the surface area, and it corresponds to the (1×1) unit cell. For Eq. (1), the entropy term TS is assumed to contribute very little to the differences in σ for the various structures, and it is, therefore, neglected at 0 K. Meanwhile, for condensed matter systems, the pressure term is negligible at low pressure. The total chemical potential of the elemental Fe and O is in equilibrium with that of bulk FeO: $\mu_{FeO}(\text{bulk}) = \mu_{Fe} + \mu_O$. Accordingly, Eq. (1) becomes

$$\sigma = (E_{\text{tot}} - N_{Fe}\mu_{FeO(\text{bulk})} + (N_{Fe} - N_O)\mu_O)/A. \quad (2)$$

The elemental Fe or O chemical potential must be less than the corresponding bulk chemical potential; otherwise, the element would form the energetically more favorable bulk structure. That is to say

$$\mu_{Fe} \leqslant \mu_{Fe(\text{bulk})}, \quad \mu_O \leqslant \mu_{O(\text{bulk})}. \quad (3)$$

Therefore, this μ_O can be varied within certain boundaries. The lower boundary for μ_O, which will be called the O-poor limit, is defined by the decomposition of the oxide into iron metal and oxygen. A reasonable upper boundary for μ_O, on the other hand (O-rich limit), is given by gas phase conditions that are so oxygen rich, that O condensation will start on the sample at low enough temperatures. Therefore, the range of the O chemical potential is[26]

$$\Delta H_f^0 \leqslant \mu_O - \mu_O^{\text{gas}} \leqslant 0, \quad (4)$$

where $\Delta H = \mu_{FeO(\text{bulk})} - \mu_{Fe(\text{bulk})} - \mu_{O(\text{gas})}$ is the 0 K formation heat of bulk FeO, which is taken to be −6.256 eV.[27] The O chemical potential is referenced with respect to the total energy of an oxygen molecule. $\Delta\mu_O = \mu_O - \mu_O^{\text{gas}} = \mu_O - (1/2)E_{O_2}^{\text{total}}$. To consider the uncertainty in these theoretically well-defined, but approximate limits for $\Delta\mu_O$, we will always plot the dependence of the surface free energies some

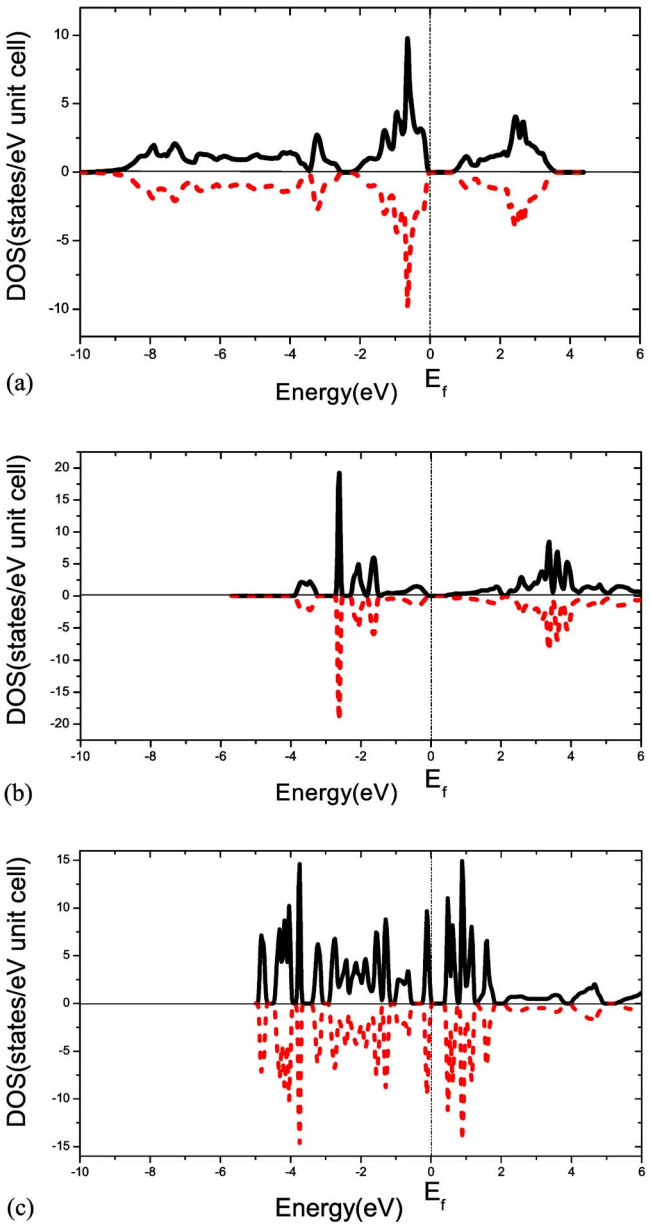

FIG. 4. (Color online) Density of states for (a) the relaxed bulk of FeO (*iB*8), (b) FeO(*iB*8)-Fe (111) surface, (c) FeO(*iB*8)-O (111) surface (dark solid: spin-up states; red dashed: spin-down states; dotted: the Fermi level).

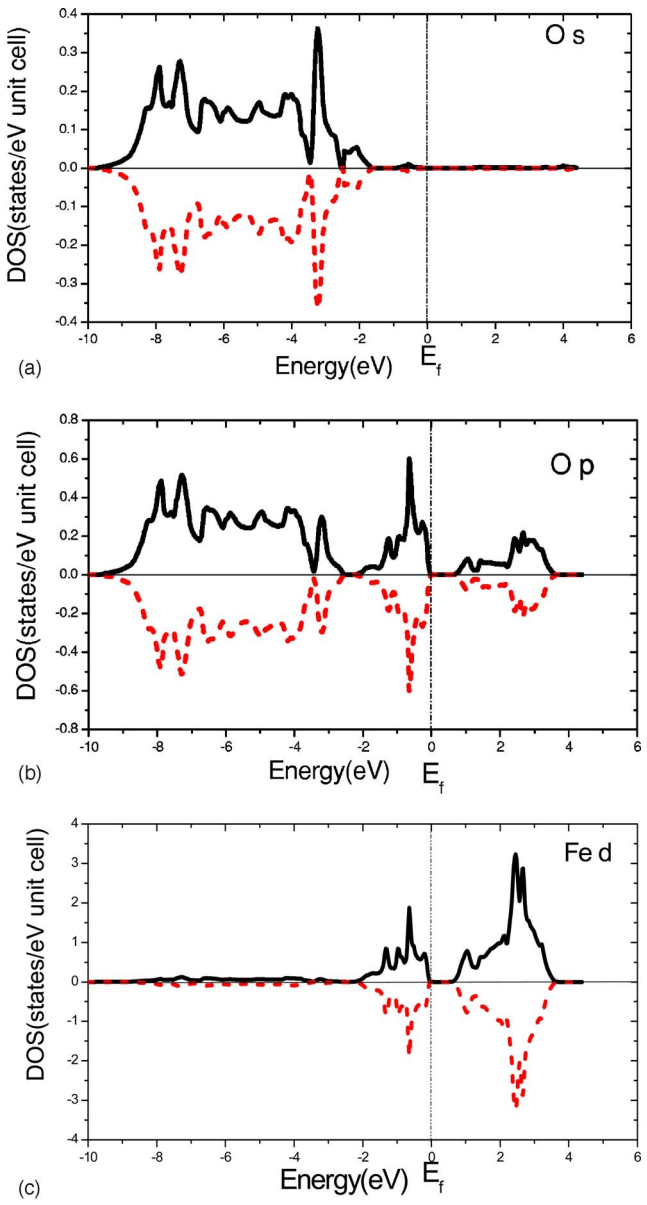

FIG. 5. (Color online) Partial density of states for FeO (*iB*8 phase) (a) *s* states of O, (b) *p* states of O, (c) *d* states of Fe (dark solid: spin-up states; red dashed: spin-down states; dotted: the Fermi level).

tenths of an eV outside these boundaries. From this it will be shown that below that the uncertainty in the boundaries does not affect at all our physical conclusions drawn.

The results of (111) surface energy (*B*1 phase) as a function of oxygen chemical potential according to Eq. (2) are given in Fig. 1. In order to compare with FeO(111), the surface energy of FeO (001) (110) is also labeled in Fig. 1.

First, the surface energies of both the Fe-terminated and O-terminated FeO(111) are relatively larger than that of the FeO (001) (110) over the whole range, especially the nonstoichiometric surface, as one expects from the polar surface. A surface with large surface energy is in a rather unfavorable state. Such a surface will lower the surface energy by large relaxation or even reconstruction as found in the relaxation of the FeO(111) surface. Meanwhile, a surface with large surface energy is generally more reactive,[28,29] which is in agreement with experiment.[30]

Second, the surface energy of FeO (001) (110) is independent of the chemical potential, while the surface energies of Fe-terminated and O-terminated FeO(111) are linearly dependent on the oxygen chemical potential. The O-terminated surface is more stable than the Fe-terminated surface at the high oxygen chemical potential $\mu_O - \mu_O^{\mathrm{gas}}$. As the oxygen chemical potential $\mu_O - \mu_O^{\mathrm{gas}}$ increases, the O-terminated surface gradually becomes more stable. Interestingly, at the high oxygen chemical potential, it is obvious that the surface energy of O-terminated FeO(111) is very close to that of FeO (110). Therefore, given enough oxygen pressure, the FeO(111) film is easily formed with the help of the texture inheritance or the film strain energy. This explains well that the FeO(111) texture can be experimentally fabricated under high oxygen pressure at a low temperature.[8]

To understand the electronic nature of these surfaces, we have calculated the density of states (DOS) of the relaxed (111) surface. Figure 2 shows the DOS of the bulk FeO (*B*1 phase), the Fe-terminated and O-terminated FeO(111) surface, where the plotted energy range is from −10 to 6 eV and the Fermi level is set to zero. As we all know, FeO (*B*1 phase) is an antiferromagnetic material with the Néel temperature of 198 K, and it behaves as an insulator.[31] From Fig. 2(a), we can see that the Fermi level of the bulk FeO (*B*1 phase) falls into the gap between the total spin-up and the spin-down bands, and the gap of the energy bands is about 3.3 eV, the value is higher than the observed band gap 2.8 eV.[32] While a drastically different situation is obtained in the structure of the Fe-terminated and the O-terminated (111) surface, the two-polar surface becomes both metallic and ferromagnetic, which is different from the bulk properties. This behavior is explained by the fact that the translational symmetry is broken at the surface.

At the same time, we also give the surface free energy of (111) (*iB*8 phase) and the surface energy of FeO (110) (*iB*8 phase) is labeled to compare with the two-polar surface in Fig. 3. We can see that the surface energy of FeO(110) surface is independent of the chemical potential, and its surface free energy is higher than the two-polar surface over the whole range, that is to say, FeO(110) surface is more active than the two-polar surface. The Fe-terminated surface is more stable than the O-terminated surface at the low oxygen chemical potential $\mu_O - \mu_O^{\mathrm{gas}}$. While as the oxygen chemical potential $\mu_O - \mu_O^{\mathrm{gas}}$ increases, the O-terminated surface gradually becomes more stable than Fe-terminated surface.

Figure 4 shows the DOS of bulk FeO with *iB*8 phase, the Fe-terminated and the O-terminated (111) polar surface, which shows that all three structures have antiferromagnetic properties and they are semiconductors. The DOS of the bulk FeO (*iB*8 phase) shows a small gap 0.52 eV, and three main regions can be observed in this figure: (i) one below −2.50 eV mainly due to oxygen 2*s* and 2*p* electrons, (ii) another between −2.39 eV and the Fermi level due to oxygen 2*p* electrons with a small contribution from Fe 3*d* electrons, and (iii) the last one between 0.52 and 3.67 eV with the biggest contribution from Fe 3*d* electrons and a smaller contribution from the other electrons, which can be seen from Fig. 5 and it shows the ionic character of the bonding.[33] For

the Fe-terminated and the O-terminated (111) surface, the gap of the energy bands are 0.35 eV 0.32 eV, respectively, which are smaller than that of the bulk FeO (*iB*8 phase).

IV. CONCLUSIONS

We have performed the LDA+U calculations with the electron correlation and the spin-orbit coupling taken into account to supplement the GGA results. The surface free energies of the (111) surface of FeO with the two possible structures (*B*1 and *iB*8 phase) were calculated. Different structures with periodicity (1×1) were fully optimized. The FeO(*B*1)-Fe and FeO(*B*1)-O surface is ferromagnetic and metallic, while the FeO(*iB*8)-Fe and FeO(*iB*8)-O surfaces show antiferromagnetic properties and are semiconductors.

ACKNOWLEDGMENTS

We acknowledge support from the National Natural Science Foundation of China under Grant Nos. 10174023, 20490210, and 10574048.

*Author to whom correspondence should be addressed. FAX: +86 27 87544525. Electronic address: klyao@hust.edu.cn
†Corresponding author. Email address: liyanli128@163.com

[1] Y. J. Kim, C. Westphal, R. X. Ynzunza, H. C. Galloway, M. Salmeron, M. A. V. Hove, and C. S. Fadley, Phys. Rev. B **55**, R13448 (1997).
[2] X. W. Zhou, H. N. G. Wadley, J-S. Filhol, and M. N. Neurock, Phys. Rev. B **69**, 035402 (2004).
[3] S.-R. Liu, Z. Dohnalek, R. S. Smith, and B. D. Kay, J. Phys. Chem. B **108**, 3644 (2004).
[4] R. Pentcheva, F. Wendler, H. L. Meyerheim, W. Moritz, N. Jedrecy, and M. Scheffler, Phys. Rev. Lett. **94**, 126101 (2005).
[5] N. F. Mott, *Metal-Insulator Transitions* (Taylor & Francis Ltd., London, 1974).
[6] M. Alfredsson, G. D. Price, C. R. A. Catlow, S. C. Parker, R. Orlando, and J. P. Brodholt, Phys. Rev. B **70**, 165111 (2004).
[7] N. C. Tombs and H. P. Rooksby, Nature (London) **165**, 442 (1950).
[8] H. C. Galloway, P. Sautet, and M. Salmeron, Phys. Rev. B **54**, R11145 (1996).
[9] J. L. Daschbach, Z. Dohnalek, S.-R. Liu, R. S. Smith, and B. D. Kay, J. Phys. Chem. B **109**, 10362 (2005).
[10] R. E. Cohen, I. I. Mazin, and D. G. Isaak, Science **275**, 654 (1997).
[11] I. I. Mazin, Y. Fei, R. Downs, and R. E. Cohen, Am. Mineral. **83**, 451 (1998).
[12] Z. Fang, I. V. Solovyev, H. Sawada, and K. Terakura, Phys. Rev. B **59**, 762 (1999).
[13] P. Blaha, K. Schwarz, G. K. H. Madsen, D. Kvasnicka, J. Luitz, WIEN2K, Vienna University of Technology, 2002, improved and updated UNIX version of the original copyrighted WIENCODE, which was published by P. Blaha, K. Schwarz, P. Sorantin, and S. B. Trickey, Comput. Phys. Commun. **59**, 399 (1990).
[14] I. I. Mazin and V. I. Anisimov, Phys. Rev. B **55**, 12822 (1997).
[15] V. I. Anisimov, J. Zaanen, and O. K. Andersen, Phys. Rev. B **44**, 943 (1991).
[16] V. I. Anisimov and O. Gunnarsson, Phys. Rev. B **43**, 7570 (1991).
[17] M. Cococcioni and S. de Gironcoli, Phys. Rev. B **71**, 035105 (2005).
[18] P. S. Bagus, C. R. Brundle, T. J. Chuang, and K. Wandelt, Phys. Rev. Lett. **39**, 1229 (1977).
[19] I. Balberg and H. L. Pinch, J. Magn. Magn. Mater. **7**, 12 (1978).
[20] Y. W. Fei and H. K. Mao, Science **266**, 1678 (1994).
[21] H. K. Mao *et al.*, Phys. Earth Planet. Inter. **96**, 135 (1996).
[22] L. M. Liu, S. Q. Wang, and H. Q. Ye, Acta Mater. **52**, 3681 (2004).
[23] D. J. Siegel, J. L. G. Hector, and J. B. Adams, Surf. Sci. **498**, 321 (2002).
[24] W. Zhang and J. R. Smith. Phys. Rev. Lett. **85**, 3225 (2000).
[25] I. G. Batyrev, A. Alavi, and M. W. Finnis. Phys. Rev. B **62**, 4698 (2000).
[26] J. Rogal, K. Reuter, and M. Scheffler. Phys. Rev. B **69**, 075421 (2004).
[27] *CRC Handbook of Chemistry and Physics*, (CRC Press, Boca Raton, FL, 1995).
[28] L. M. Liu, S. Q. Wang, and H. Q. Ye, J. Phys.: Condens. Matter **15**, 8103 (2003).
[29] D. J. Siegel, J. L. G. Hector, and J. B. Adams, Phys. Rev. B **67**, 092105 (2003).
[30] K. Koike and T. Furukawa, Phys. Rev. Lett. **77**, 3921 (1996).
[31] M. R. Norman. Phys. Rev. B **44**, 1364 (1991).
[32] S. Masuda, Y. Harada, H. Kato, K. Yagi, T. Komeda, T. Miyano, M. Onchi, and Y. Sakisaka. Phys. Rev. B **37**, 8088 (1988).
[33] N. Takeuchi. Phys. Rev. B **66**, 153405 (2002).